

Vibrational relaxation pathways in porous silicon: A time-resolved infrared spectroscopic studyK. W. Jobson,^{1,*} J.-P. R. Wells,¹ N. Q. Vinh,² P. J. Phillips,^{2,3} C. R. Pidgeon,³ and J. I. Dijkhuis⁴¹*Department of Physics and Astronomy, University of Sheffield, Sheffield S3 7RH, United Kingdom*²*FELIX Free Electron Laser Facility, FOM Institute for Plasmaphysics 'Rijnhuizen', P.O. Box 1207, 3430 BE, Nieuwegein, The Netherlands*³*Department of Physics, Heriot-Watt University, Riccarton, Edinburgh, United Kingdom*⁴*Department of Physics and Astronomy, University of Utrecht, P.O. Box 80000, TA 3508 Utrecht, The Netherlands*

(Received 16 June 2006; published 19 October 2006)

We have used a free electron laser to measure the picosecond vibrational dynamics of the SiH, SiH₂, and O₃SiH stretching modes in porous silicon. A three beam pump-probe technique has been employed to make temperature dependent measurements of the population relaxation times. We demonstrate that both bending modes and scissors modes play important roles as does the vibrational bath provided by the pore walls themselves. Using a forward box, two beam photon echo technique we have measured the homogeneous dephasing times of all modes which have dynamic linewidths in the range 0.6–1.2 cm⁻¹. The inferred pure dephasing rates are dominated by the elastic scattering of acousticlike Si-Si vibrations.

DOI: [10.1103/PhysRevB.74.165205](https://doi.org/10.1103/PhysRevB.74.165205)

PACS number(s): 78.47.+p, 63.50.+x, 81.05.Rm

I. INTRODUCTION

Direct ultrafast time-resolved measurements of both vibrational lifetimes and vibrational coherent transients such as photon echoes, are a relatively recent development which have been made possible due to advances in the generation of subpicosecond infrared pulses in the 3–20 micron, “molecular fingerprint” region. In particular, we highlight the increasing availability of beamtime at free electron laser (FEL) user facilities as well as the development of infrared optical parametric amplifiers. Thus far, rather few groups around the world have focused on time resolved vibrational spectroscopy of point defects in solids and it is often deemed an emerging field. There have been several reports of time-resolved studies made on SiH defects in different environments, an overview of which can be found in Lüpke *et al.*¹ These experiments have shown that the structure of the localized vibrational mode’s surrounding environment has profound consequences for the anharmonic decay of fundamental localized vibrational modes. Our work has covered vibrational decay pathways² and free induction decay and vibrational ladder climbing³ of H⁻ local modes in insulating crystals and extensive studies of SiH/D and Si-O-Si stretching modes in amorphous silicon (*a*-Si).^{4–6} These works have shown that the disordered environment of an amorphous host can lead to a nonexponential population relaxation if the appropriate combination of accepting modes includes internal modes of the defect such as bending modes. This has also been shown to be true in hydrogenated amorphous germanium (*a*-Ge:H).⁷

In this paper, we report on three beam, infrared pump probe and photon echo experiments performed resonant with the stretching modes of the SiH, SiH₂, and O₃SiH defects in free standing porous silicon (*p*-Si). Porous silicon consists of a wafer of bulk *c*-Si into which a series of pores are electrochemically etched. The disordered surfaces of these walls are passivated by hydrogen, supplied by the HF solution used in the etching process. This results in pore walls which are coated with various hydrogenic species (e.g., SiH, SiH₂,

SiH₃), dangling bonds and also some oxide species. The particularly interesting aspect of this, from a vibrational dynamics point of view, is that although the SiH defect resides in a locally disordered environment, the silicon beyond the pore walls retains its crystalline structure and so the long-wavelength bulk vibrations are crystalline in character. This can be seen in the Raman spectra of *p*-Si,⁸ where sharp crystalline peaks are observed on top of the broadened amorphous peaks. Therefore vibrational relaxation of the SiH modes in *p*-Si is an interesting case to study, in that it is uncertain as to whether the vibrations relax to the delocalized bulk crystalline phonons or conversely, couple to the local amorphous vibrational bath.

II. EXPERIMENT

The samples consist of electrochemically prepared, free standing *p*-Si. The layers are ~130 μm thick and were prepared from a *c*-Si wafer. The infrared absorption spectrum of the sample was measured with a nitrogen purged Nicolet FTIR spectrometer. The time resolved measurements were performed using the Dutch free electron laser FELIX in Nieuwegein. The output of FELIX consists of a train of “macropulses” ~4 μs in length running at a repetition rate of 5 Hz. Each macropulse is made up of “micropulses.” The micropulses, which provide the time resolution of the measurements, have a width which is adjustable between 300 fs and 10 ps with a pulse separation of 40 ns. FELIX is continuously tunable from 3.9 to 250 μm and more than adequately covers the 4.3–5 μm region of immediate interest. In each case FELIX was tuned to be resonant with the vibrational mode in question.

The population relaxation was measured using a three beam, balanced pump-probe experiment⁹ in which the input FELIX beam is split into pump, probe, and reference beams using BaF₂ beam splitters. The reference pulse is sent down a 6 meter arm and then back reflected onto the probe pulse path. Therefore the probe and reference beams follow the same optical path, travel through the sample at the same

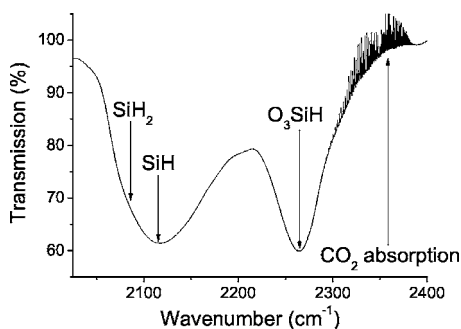


FIG. 1. Infrared transmission spectrum of a free-standing *p*-Si layer. The spectral positions of the SiH, SiH₂, and O₃SiH mode are highlighted. The sharp lines observed on the high energy side of the spectrum are due to CO₂ absorption.

position and are detected by the same mercury cadmium telluride (MCT) detector. MCT detectors are commonly operated at constant bias, however in this experiment the bias was modulated synchronously with the 25 MHz FELIX micropulse repetition rate. When the system is in balance, the integrating electronics give an apparent output signal of zero. The three beams were focused onto the sample with a 90° off axis parabolic mirror having a focal length of 15 cm. Temperature control was provided by the use of an Oxford Instruments “Microstat” cold finger cryostat equipped with a model ITC503 controller.

The photon echo measurement is a standard coherent transient technique¹⁰ which in its simplest form utilizes a two pulse sequence in a transmission geometry. The power of the echo technique lies in its ability to eliminate the inhomogeneous broadening contribution to the total linewidth thereby providing a direct measurement of homogeneous dephasing. The first pulse (having wave vector \mathbf{k}_1) creates a coherent admixture of vibrational states whose initial phase is lost due to free induction decay. The second pulse (with wave vector \mathbf{k}_2) inverts the macroscopic dipole yielding a phase matched super-radiant burst which is known as a photon echo. The time integrated echo signal propagating along the $\mathbf{k}_{\text{echo}} = |\mathbf{2k}_2 - \mathbf{k}_1|$ signal direction decays as a function of the delay between the incoming pulses as $T_2/4$. The key feature of the photon echo technique is that it exploits the fact that the free induction decay is reversible.

III. RESULTS

Figure 1 presents the infrared transmission spectrum of porous silicon, truncated to show only the 2025–2400 cm⁻¹ region of interest. With reference to the many infrared investigations of *p*-Si that exist in the literature,^{11,12} we assign the broad peak at 2114 cm⁻¹ as the $\nu=0 \rightarrow 1$ SiH stretching mode. A shoulder at 2083 cm⁻¹ arises from the SiH₂ species. The more isolated absorption feature at 2262 cm⁻¹ is due to the fundamental stretch vibration of SiH bonds where the Si atom is backbonded to O atoms.¹³ This feature is only observed in oxidized *p*-Si (Ref. 14) and comes from oxygen preferentially attacking the weaker Si-Si backbonds of the SiH defect. Both the bending mode (at 878 cm⁻¹) and stretching mode of the oxygen backbonded SiH defect has a

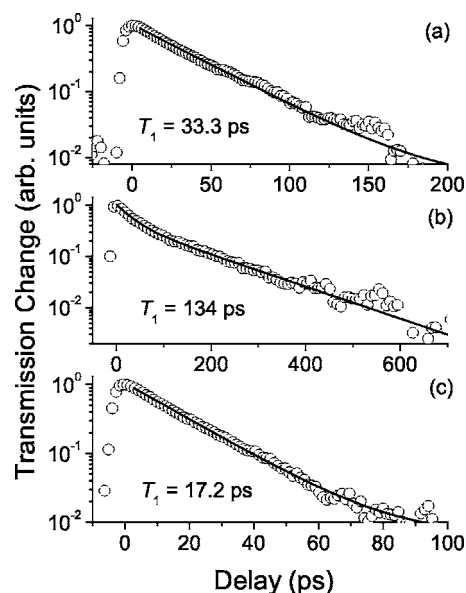


FIG. 2. Decay of the pump-probe signals at a temperature of 10 K when resonantly exciting the SiH stretch mode at (a) 4.73 μm , the SiH₂ stretch mode at (b) 4.80 μm , and the oxygen backbonded SiH stretch mode at (c) 4.42 μm . The solid lines are fits of single-exponential decay in cases (a) and (c), while in case (b) a biexponential fit is used. The lifetimes of the respective modes, obtained through these fits, are indicated.

higher frequency compared to the other two modes, due to the highly electronegative O atoms pulling the electron cloud away from the Si atom.

A. Lifetime measurements

Figures 2(a)–2(c) show the pump-probe signals measured at 10 K for all three vibrational modes. Resonant excitation of the SiH and O₃SiH stretch modes [Figs. 2(a) and 2(c)] is observed to yield single-exponential decay with decay constants of $T_1=33.3$ ps and $T_1=17.2$ ps, respectively. Figure 2(b) shows the pump-probe signal for resonant excitation of the SiH₂ stretching mode. The measured response is well approximated by a biexponential relaxation and has a long time component which is considerably longer than the lifetimes measured for the SiH and O₃SiH modes. We have established that the biexponential behavior is due to both the SiH and SiH₂ modes being simultaneously excited by the FELIX pulse. Thus we find that by fitting a bi-exponential curve to the data, the faster decaying component has a lifetime of 29.3 ps, which corresponds well within the accuracy of the measurement to the decay time of the SiH mode and that the longer decaying component has a decay time of 134 ps and this is the lifetime of the SiH₂ stretch mode.

The overall behavior observed differs from *a*-Si:H in one important respect, which is that in *p*-Si the stretch mode dynamics are observed to have single exponential relaxation while in *a*-Si:H a distribution of lifetimes is measured.^{4,15,16} This is caused by the distribution of bond angles and bond lengths that are characteristic of the random network structure of amorphous solids, coupled to the highly localized

nature of the SiH defect. These two characteristics cause a local change in the coupling of each SiH defect to the Si-Si phonon bath, thus leading to a distribution of decay rates. The absolute value of the relaxation rate of the SiH stretch mode is a factor of four larger than observed in *a*-Si (Refs. 4 and 16) and is due to better coupling to the surroundings in *p*-Si. We note that time-resolved transient bleaching experiments performed upon the stretch mode of bond center H in *c*-Si measured a decay time of $T_1=7.8$ ps.¹⁷ Both interstitial hydrogen defects as well as hydrogen vacancy complexes appear to have 10 K lifetimes in the range ~ 2 –40 ps, comparable with our observations for *p*-Si. Time-resolved measurements of the vibrational population decay of the SiH stretch mode of an H-terminated *c*-Si surface¹⁸ also showed a single-exponential decay, but over a greatly-increased time-scale ($T_1 \sim 1$ ns), attributable to extremely weak coupling of the stretch mode to other internal defect modes as well as the surrounding phonon bath. This suggests that in *p*-Si the local environment of the Si-H is markedly different than that of both *a*-Si and *c*-Si.

The temperature dependence of the decay rate of the anharmonic decay of a localized mode of frequency ω into a set of accepting modes of frequencies ω_i can be modeled with the expression¹⁹

$$[T_1(T)]^{-1} = [T_1(0)]^{-1} \left(\frac{\exp(\hbar\omega/k_B T) - 1}{\prod_i [\exp(\hbar\omega_i/k_B T) - 1]} \right), \quad (1)$$

where $[T_1(0)]^{-1}$ is the 0 K population decay rate (which we reasonably approximate with data measured at 10 K) and $\sum_i \hbar\omega_i = \hbar\omega$ in order to satisfy energy conservation. Figures 3(a)–3(c) present the measured temperature dependence of the decay rate of the three modes of interest and we discuss each in turn.

1. SiH stretch mode

Figure 3(a) shows the temperature dependence of the decay rate for the SiH stretch mode at 2114 cm^{-1} , which is observed to increase by a factor of ~ 1.4 from 10 K to room temperature. The dashed-dotted curve, which overestimates the data at temperatures above 150 K, represents decay into five equal energy 423 cm^{-1} Si-Si vibrations. Any alternative five phonon choice gives an increasingly degraded account of the data. Assuming four phonon decay into energy-degenerate Si-Si vibrations at 529 cm^{-1} is shown by the dotted line and badly underestimates the data. The dashed curve assumes anharmonic decay to one SiH bending mode [at 625 cm^{-1} (Ref. 11)] with the energy surplus bridged by two 530 cm^{-1} and one 429 cm^{-1} Si-Si vibration. This also underestimates the data. The solid line represents decay into two bending modes, one 530 cm^{-1} and a 334 cm^{-1} Si-Si vibration, giving good account of the data. In *a*-Si the SiH stretch decay path is via three bending modes and one 133 cm^{-1} phonon,^{4,16} suggesting that in *p*-Si, the vibrational coupling of the Si-H stretch mode to the Si-Si TO and LA lattice modes is enhanced.

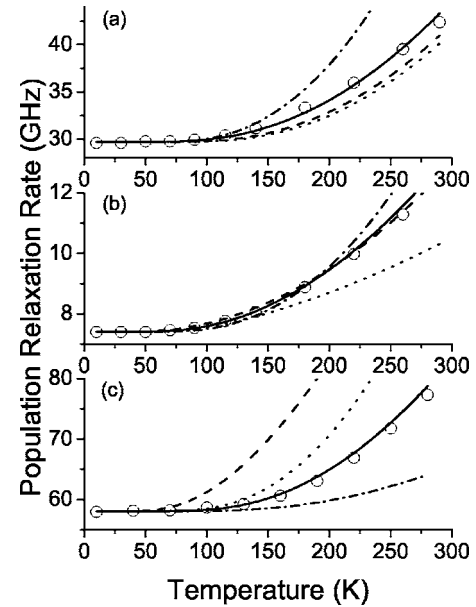


FIG. 3. Temperature dependence of the population relaxation rate $1/T_1$ of (a) the SiH stretch mode, (b) the SiH₂ stretch mode, and (c) the O₃SiH mode. The circles are the measured lifetimes while the lines are fits of Eq. (1) in which either three-, four-, or five-phonon anharmonic decay with appropriate choices of Si-Si vibrational energy are used. In case (a) (Si-H) the best fit is the unbroken line, which represents four-phonon decay into two bending modes (625 cm^{-1}), and two Si-Si vibrations at 530 cm^{-1} and 334 cm^{-1} . For case (b) (Si-H₂), there are two equally plausible decay pathways, shown as the unbroken and dashed line. The unbroken line assumes four-phonon decay into one scissors mode (906 cm^{-1}) and three bulk vibrations having energies of 530 cm^{-1} , 370 cm^{-1} , and 275 cm^{-1} . The dashed curve also assumes four-phonon decay with the accepting modes being two bending modes (660 cm^{-1}) and two Si-Si vibrations having energies of 530 cm^{-1} and 233 cm^{-1} . In the last case (c) (O₃Si-H) the best fit is the unbroken line and assumes four-phonon decay into one bending mode (625 cm^{-1}) and three equal energy 461 cm^{-1} vibrations. Full details of the various energy conserving phonon decay pathways are given in the text.

2. SiH₂ stretch mode

Figure 3(b) shows the temperature dependent decay rate of the SiH₂ stretch mode at 2083 cm^{-1} . The measured decay rates increase by a factor of ~ 1.5 from 10 K to 250 K. The dashed-dotted curve represents anharmonic decay into five equal energy 417 cm^{-1} Si-Si vibrations. This both underestimates the data in the 100–200 K range and overestimates the data at higher temperatures, although not significantly. We note that the SiH₂ defect has both a scissors mode at 906 cm^{-1} and a bending mode at 660 cm^{-1} .¹¹ The closest three-phonon decay possibility is shown as the dotted curve, representing decay via two scissors modes and a 267 cm^{-1} Si-Si vibration. This approximation does not account for the data very well, falling well behind the measured decay rates at temperatures higher than 150 K. The two “best choice” approximations are both four-phonon decay processes. The solid line is decay via one scissors mode and three Si-Si vibrations at 530 cm^{-1} , 370 cm^{-1} , and 275 cm^{-1} . An equally

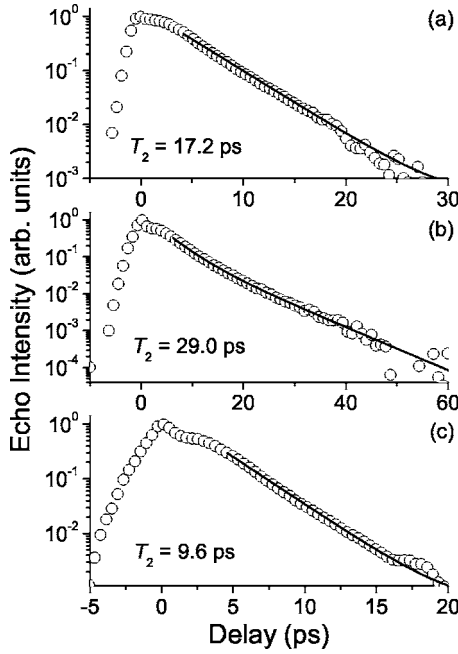


FIG. 4. Decay of the photon echo signals at a temperature of 10 K when resonantly exciting (a) the SiH stretch mode at $4.73 \mu\text{m}$, (b) the SiH₂ stretch mode at $4.80 \mu\text{m}$, and (c) the oxygen backbonded SiH stretch mode at $4.42 \mu\text{m}$. In cases (a) and (c) the lines are single-exponential fits to the measured decay of the echo. In case (b) a biexponential fit is used. The respective dephasing times of each mode are displayed in the corner of each plot.

valid alternative is relaxation via two bending modes and two Si-Si vibrations at 530 cm^{-1} and 233 cm^{-1} (dashed curve). It is not possible, within the accuracy of the measurements, to distinguish between these two possibilities. As for the SiH stretch mode in *p*-Si, the coupling to the Si-Si TO and TA lattice modes seems to limit the vibrational lifetime of the SiH₂ stretch mode.²⁰

3. O₃SiH stretch mode

Figure 3(c) shows the temperature dependent decay rates for the O₃SiH stretch mode at 2262 cm^{-1} , whose decay rate increases by a factor of ~ 1.4 between 10 K and room temperature. As expected, attempts to account for the data in terms of five phonon decay vastly overestimate the measured decay rates. This is shown as a dotted curve for five 452 cm^{-1} Si-Si vibrations. Nor does three phonon decay give reasonable account of the data due to the high energy of the accepting modes required. The dashed-dotted curve represents decay into two bending modes at 878 cm^{-1} and a 506 cm^{-1} Si-Si vibration. Conversely, assuming four-phonon decay into two bending modes and two 253 cm^{-1} Si-Si vibrations (shown as the dashed line) vastly overestimates the increase in relaxation rate. We find that the best account of the data is given by decay into one bending mode and three vibrations at 461 cm^{-1} (shown as the solid line). We note that *p*-Si has a IR strong absorbance at 460 cm^{-1} related to Si-O-Si bending vibrations,²⁰ suggesting that a resonant coupling to this mode speeds up the relaxation of the O₃SiH stretch mode.

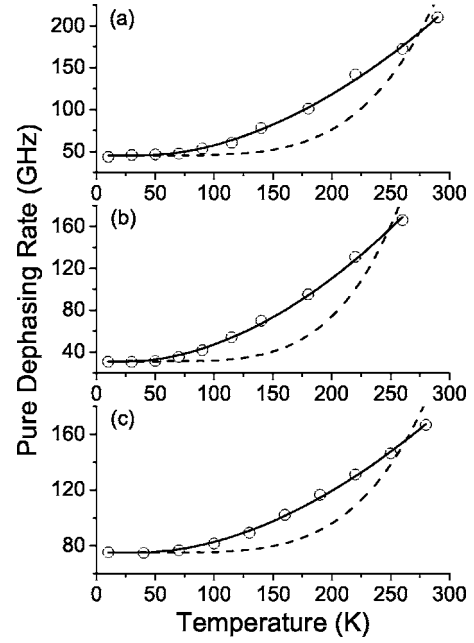


FIG. 5. Temperature dependence of the pure dephasing rate of (a) the SiH stretch mode, (b) the SiH₂ stretch mode, and (c) the O₃SiH mode. The dashed line is a least-squares fit to Eq. (2) and the solid line is a least-squares fit to Eq. (3).

We have shown that in *p*-Si for all three defects, the stretching mode relaxes to internal localized modes, such as scissors or bending modes, and that for the SiH and SiH₂ stretch modes energy conservation is satisfied via the phonon bath.

B. Dephasing measurements

Figures 4(a)–4(c) show the photon echo obtained for the SiH, SiH₂, and O₃SiH stretch modes as measured at 10 K. At all wavelengths a so-called “coherent spike” at zero delay is observed. From these transients we infer homogeneous dephasing times of $T_2 = 17.2 \text{ ps}$ (SiH), $T_2 = 29.0 \text{ ps}$ (SiH₂), and $T_2 = 9.6 \text{ ps}$ (O₃SiH) yielding homogeneous (dynamic) linewidths ($1/\pi T_2$) of 0.62 cm^{-1} , 0.37 cm^{-1} , and 1.1 cm^{-1} , respectively. Comparison with the linewidths as measured by FTIR spectroscopy confirms that there is massive inhomogeneous broadening arising from the disordered environment.

The homogeneous dephasing rate (T_2^{-1}) measured using the photon echo technique has contributions from the population relaxation rate (T_1^{-1}) and the pure dephasing rate (T_2^{*-1}). Pure dephasing is an adiabatic process giving rise to fluctuations in the vibrational eigenstates. The various contributions are connected via the well known expression $1/T_2 = 1/2T_1 + 1/T_2^*$.¹⁰ By combining the population relaxation rates and homogeneous dephasing rates, the pure dephasing rate can be extracted. Figures 5(a)–5(c) display the temperature dependence of the pure dephasing rate for all three modes. We interpret the temperature dependent pure dephasing as arising from elastic scattering of Si-Si band phonons. Under the assumption of a Debye-like density of states, this takes the analytical form

$$[T_2^*(T)]^{-1} = a + A \left(\frac{T}{\Theta_D} \right)^7 \int_0^{\Theta_D/T} \frac{x^3}{e^x - 1} dx, \quad (2)$$

where a is a constant added to account for the finite dephasing at cryogenic temperatures, A is a coupling constant, and Θ_D is the Debye temperature (here taken to be $\Theta_D = 487$ K, see Ref. 21). As can be seen from Figs. 5(a)–5(c), where the Debye approximation is plotted as a dashed line, this assumption completely underestimates the activation of the pure dephasing rate with temperature for all three modes. A common alternative assumption is that the pure dephasing is dominated by a single Si-Si vibrational mode yielding

$$[T_2^*(T)]^{-1} = a + An_\omega(n'_\omega - 1), \quad (3)$$

where n_ω is the Bose-Einstein occupation factor for the appropriate mode's energy. This is shown as a solid line in Figs. 5(a)–5(c) and yields good agreement with the data. The coupling constant of the three defects is found to be within the same order of magnitude for each mode, ranging from (a) 147 GHz (SiH), (b) 71 GHz (SiH₂), and (c) 80 GHz (O₃SiH), while the corresponding phonon energies are (a) 184 cm⁻¹, (b) 128 cm⁻¹, and (c) 175 cm⁻¹. Thus the pure dephasing of all three modes is dominated by elastic scattering from long-wavelength Si-Si vibrations.

IV. SUMMARY

We present results of picosecond vibrational dynamics experiments for the SiH, SiH₂, and O₃SiH stretch modes in *p*-Si. We find that the vibrational population decay for each mode is single exponential. The temperature dependent population relaxation rate of the SiH and SiH₂ stretch modes show that the vibrational energy is quickly drained to lower energy internal vibrational modes with excess energy taken up by Si-Si TO and LA lattice modes. The vibrational decay channel of the O₃SiH stretch mode is quite efficient, presumably of resonant local character, and governed by bending vibrations. Photon echo experiments confirm that the high frequency stretch modes experience massive inhomogeneous broadening. The temperature dependent pure dephasing is dominated by elastic scattering of low frequency “acoustic-like” vibrations.

ACKNOWLEDGMENTS

K.W.J. would like to thank the EU for the provision of funds to travel to FELIX and undertake this work. The authors acknowledge the support of the Dutch FOM (Stichting voor Fundamenteel Onderzoek der Materie) organization in providing the required beamtime on FELIX as a part of the FOM-EPSRC agreement.

*Corresponding author: K. W. Jobson. Email address: k.jobson@sheffield.ac.uk

- ¹G. Lüpke, N. H. Tolk, and L. C. Feldman, *J. Appl. Phys.* **93**, 2317 (2003).
- ²J.-P. R. Wells, I. V. Bradley, G. D. Jones, and C. R. Pidgeon, *Phys. Rev. B* **64**, 144303 (2001).
- ³J.-P. R. Wells, C. W. Rella, I. V. Bradley, I. Galbraith, and C. R. Pidgeon, *Phys. Rev. Lett.* **84**, 4998 (2000).
- ⁴M. van der Voort, C. W. Rella, L. F. G. van der Meer, A. V. Akimov, and J. I. Dijkhuis, *Phys. Rev. Lett.* **84**, 1236 (2000).
- ⁵J.-P. R. Wells, R. E. I. Schropp, L. F. G. van der Meer, and J. I. Dijkhuis, *Phys. Rev. Lett.* **89**, 125504 (2002).
- ⁶J.-P. R. Wells, P. J. Phillips, N. Tomozeiu, F. H. P. M. Habraken, and J. I. Dijkhuis, *Phys. Rev. B* **68**, 115207 (2003).
- ⁷K. W. Jobson, J.-P. R. Wells, R. E. I. Schropp, D. A. Carder, P. J. Phillips, and J. I. Dijkhuis, *Phys. Rev. B* **73**, 155202 (2006).
- ⁸Z. Sui, P. P. Leong, I. P. Herman, G. S. Higashi, and H. Temkin, *Appl. Phys. Lett.* **60**, 2086 (1992).
- ⁹P. C. Findlay, C. R. Pidgeon, R. Kotitschke, A. Hollingworth, B. N. Murdin, C. J. G. M. Langerak, A. F. G. van der Meer, C. M. Ciesla, J. Oswald, A. Homer, G. Springholz, and G. Bauer, *Phys. Rev. B* **58**, 12908 (1998).
- ¹⁰K. D. Rector and M. D. Fayer, *Int. Rev. Phys. Chem.* **17**, 261 (1998).

- ¹¹W. Theiß, *Surf. Sci. Rep.* **29**, 91 (1997).
- ¹²J. A. Glass Jr., E. A. Wovchko, and J. T. Yates Jr., *Surf. Sci.* **348**, 325 (1995).
- ¹³M. A. Butturi, M. C. Carotta, G. Martinelli, L. Passari, G. M. Youssef, A. Chiorino, and G. Ghiotti, *Solid State Commun.* **101**, 11 (1997).
- ¹⁴D. B. Mawhinney, J. A. Glass Jr., and J. T. Yates Jr., *J. Phys. Chem. B* **101**, 1202 (1997).
- ¹⁵Z. Xu, P. M. Fauchet, C. W. Rella, H. A. Schwetman, and C. C. Tsai, *J. Non-Cryst. Solids* **198**, 11 (1996).
- ¹⁶C. W. Rella, M. van der Voort, A. V. Akimov, A. F. G. van der Meer, and J. I. Dijkhuis, *Appl. Phys. Lett.* **75**, 2945 (1999).
- ¹⁷M. Budde, C. Lüpke, C. P. Cheney, N. H. Tolk, and L. C. Feldman, *Phys. Rev. Lett.* **85**, 1452 (2000).
- ¹⁸P. Guyot-Sionnest, P. Dumas, Y. J. Chabal, and G. S. Higashi, *Phys. Rev. Lett.* **64**, 2156 (1990).
- ¹⁹A. Nitzan, S. Mukamel, and J. Jortner, *J. Chem. Phys.* **60**, 3929 (1974).
- ²⁰H. D. Fuchs, M. Stutzmann, M. S. Brandt, M. Rosenbauer, J. Weber, A. Breitschwerdt, P. Deak, and M. Cardona, *Phys. Rev. B* **48**, 8172 (1993).
- ²¹B. L. Zink, R. Pietri, and F. Hellman, *Phys. Rev. Lett.* **96**, 055902 (2006).